In Situ Polymerization of the 4-Vinylbenzenesulfonic Anion in Ni−Al−Layered Double Hydroxide and Its Molecular Dynamic Simulation

Dongpeng Yan,[†] Jun Lu,[†] Min Wei,*[,†] Hui Li,[‡] Jing Ma,[‡] Feng Li,[†] David G. Evans,[†] and Xue Duan[†]

State Key Laboratory of Chemical Resource Engineering, Beijing University of Chemical Technology, Beijing 100029, P. R. China, and Institute of Theoretical and Computational Chemistry, Key Laboratory of Mesoscopic Chemistry of MOE, Nanjing University, Nanjing 210093, P.R. China

Received: March 4, 2008; Revised Manuscript Received: June 21, 2008

This paper describes a systematic study on the thermal polymerization of both pristine 4-vinylbenzenesulfonic anion (VBS) and intercalated VBS in the two-dimensional (2D) gallery of Ni−Al layered double hydroxide (VBS/Ni−Al-LDH), by virtue of combining experimental and theoretical investigations. In situ FT-IR, in situ high-temperature X-ray diffraction (HT-XRD), UV−vis absorption spectroscopy, TG-DTA and elemental analysis were used to study the polymerization process, and it was found that the polymerization of VBS/Ni−Al-LDH occurs at ca. 150−170 °C, at least 40 °C lower than that of the pristine VBS, indicating that the layered structure of LDH is favorable for thermal polymerization of VBS. Therefore, this layered inorganic material may have potential application as a "molecular reactor" for enhancing the efficiency of polymerization reaction. Furthermore, the sheet-like polymerization product was obtained with the LDHs lamella as template. For better understanding the structure and arrangement of intercalated VBS and the polymerization product between the layers of Ni−Al-LDH, molecular dynamics (MD) simulation method was employed. The simulation results of hydration energies show that there are two relatively stable stages upon the increase of the number of interlayer water molecules. VBS molecules exhibit a tendency from tilted to vertical orientation with respect to the layers as the interlayer water content increases. Compared with the experimental results, the calculated interlayer spacing is more severely affected by interlayer water content. Finally, a typical tetramer product of VBS intercalated LDH was studied and the simulated equilibrium interlayer spacing is consistent with the experimental result of in situ HT-XRD. Based on the combination of experimental and theoretical studies on the interlayer polymerization system, the aim of this work is to deeply investigate the differences in thermal polymerization process between pristine monomers and intercalated ones in the gallery of LDHs, and to give detailed information of the arrangement and swelling behavior of guest molecules confined between the sheets of host layers.

Introduction

Layered double hydroxides (LDHs), are a large type of naturally occurring and synthetic materials, which can be described by the general formula: $[M^{II}_{1-x}M^{III}_{x}(OH)_2]^{z+}A^{n-}_{z/n}\cdot yH_2O$. M^{II} and M^{III} are divalent and trivalent metals, respectively; A^{n-} is the anion which compensates for the positive charges of the hydroxide layers, and the interlayer anion can also be exchanged by other inorganic or organic anions. LDHs materials present a large variety of advantages, such as tunable charge density of the layer, anion exchange behavior, memory effort, and so on. In the past two decades, many potential applications of LDHs have been studied in the areas of catalysis,[1,2] separation technology,[3,4] drug delivery,[5,6] and optical materials.[7,8] Moreover, LDHs can be a special "molecular reactor" for the novel 2D confined molecular reactions, which has been applied to control the growth of nanocrystals,[9] or to control the distribution of products.[10] Furthermore, syntheses of organic−inorganic hybrid materials based on LDHs have attracted much attention of researchers, for these materials may show some special physicochemical characteristics compared with the individual parts.

Polymer/LDHs system is an important part of organic−inorganic hybrid materials. Schöllhorn et al.[11] reviewed three main pathways to obtain the polymer intercalated layered inorganic host, one of which was in situ polymerization including oxidation method and thermal polymerization directly. Based on this method, syntheses and characterizations of various anionic polymer/LDHs nanocomposites were further reported (e.g., polyaniline sulfonate,[12] polysulfopropyl methacrylate (SPMA),[13] polyacrylate[14]). In situ polymerization of the 4-vinylbenzenesulfonic anion (VBS) in the gallery of LDHs has been widely studied by Leroux et al.[15–18] They have compared the thermal behavior of VBS/Zn−Al-LDH under N_2 with that of under air conditions by the use of EXAFS and XANES method. The textural and electrochemical properties of carbon replica obtained from pyrolysis of VBS/LDH were also studied. To the best of our knowledge, the comparison study on differences of in situ thermal polymerization process between pristine monomers and intercalated ones in the gallery of LDHs has seldom been carried out, and the morphology of the polymerization products obtained from the layers has not been reported. Moreover, the arrangement and orientation of monomer molecules, which are key factors for polymerization, are

* Corresponding author. Phone: +86-10-64412131. Fax: +86-10-64425385. E-mail: weimin@mail.buct.edu.cn.
[†] Beijing University of Chemical Technology.
[‡] Nanjing University.

10.1021/jp801922b CCC: $40.75
Published on Web 07/25/2008

not further investigated. These may largely restrict the understanding of the different polymerization behaviors of monomers between the confined and bulk reaction conditions.

In recent years, because the experimental characterizations are limited for further understanding the structure of materials, the theoretical computational method has been an important technique to study and predict the properties beyond experimental observations. Molecular simulation is one of the important tools of computational chemistry, which has the advantage for dealing with much larger systems than quantum mechanical calculations. Classical molecular simulation methods, mainly consisting of Monte Carlo (MC) and molecular dynamic (MD) techniques, are widely used to investigate structures and properties of anionic and cationic clays. Greenwell et al.[19] reviewed a number of molecular simulation details and results for these two clay species. As we have known, during the past 10−15 years, MC simulation was mainly performed for the system of cationic clay (e.g., smecties),[20–22] whereas MD simulation was used for both of them and provided an effective and complementary method to investigate the important properties of these clay materials, e.g., self-diffusion coefficients, radial distribution functions (RDFs) of the ions between the host layers. The MD simulation method has also been employed to study structures and properties of various organic and inorganic molecules intercalated LDHs.[23–33] The hydration energies in several different systems were calculated for predicting the swelling behavior of clays.[26,32,33] Wang et al.[26] reported that there was a clear minimum of hydration energy that corresponds to the state observed in experiments for the study of Cl^-/LDH, whereas Kumar et al.[32] concluded that there was no preferred hydration state in citrate intercalated LDH. The interlayer spacing as a function of water content was also widely studied,[24,26,31–33] unfortunately, the variation of interlayer spacing upon the increase of hydration state was seldom to be compared with that of experimental results except for Newman et al.'s work.[24] The arrangement and orientation of anions within the layers, such as carboxymethyl β-cyclodextrin (β-CMCD)[29] and some drug molecules,[30] were also probed. To the best of our knowledge, most of MD simulation studies were mainly focused on the system of Mg−Al-LDH, and several force fields are improved and modified, such as Dreiding force field,[23,34] CVFF force field,[35] and CLAYFF force field.[27] Recently, we have developed a modified cff91 force field for Ni−Al-LDH and investigated the relative ion-exchange abilities of different anions.[31] The simulation results fit very well with the experimental ones, which show the validity of the modified force field for Ni−Al-LDH system.

In the present work, the detailed polymerization processes for both pristine VBS and VBS intercalated Ni−Al-LDH have been investigated by comparing the differences between the bulk and confined reaction, and the sheet-like polymerization product in the confined region was obtained with the LDHs lamella as template. Moreover, we employed the modified cff91 force field to perform MD simulation for analyzing structures and properties (e.g., the swelling properties, geometries and orientations) of VBS and its interlayer polymerization product confined between the layers of Ni−Al-LDH. The results of theoretical study are in approximately agreement with those of the experimental ones, demonstrating the feasibility of MD simulation for this system. Therefore, this work not only gives a further insight into how the confined region influences the thermal polymerization of guest monomers in terms of experiments but also provides a detailed understanding of the arrangement styles of monomers and products confined between the sheets of LDHs by theoretical calculations. It can be expected that this layered inorganic materials could be applied to impose restricted geometry on the interlayer confined reaction leading to enhanced control of product morphology and distribution.

Experimental Section

Materials. Sodium vinylbenzene-4-sulfonate (VBS, >90%) and polystyrenesulfonate (PSS, $M_w = 700000$) were purchased from Sigma Chemical Co. Ltd. NaOH, $Ni(NO_3)_2 \cdot 6H_2O$ and $Al(NO_3)_3 \cdot 9H_2O$ were purchased from Beijing Chemical Co. Ltd. and used without further purification.

Preparation of VBS/LDH and PSS/LDH. VBS monomer intercalated Ni−Al-LDH was prepared by the coprecipitation method,[36] which is the most common preparation method of LDHs. The matched molar ratio of $Ni^{2+}/Al^{3+}/OH^-$/VBS was 2.0:1.0:6.0:3.0 in this experiment. A solution of $Ni(NO_3)_2 \cdot 6H_2O$ (0.05 mol) and $Al(NO_3)_3 \cdot 9H_2O$ (0.025 mol) in 100 mL of deionized water was slowly added dropwise to a solution of NaOH (0.15 mol) and VBS (0.075 mol) in 100 mL of deionized water with vigorous agitation under a nitrogen flow. The value of the pH at the end of addition was adjusted to 8.0 by further addition of 2.4 mol/L NaOH solution. The reaction mixture was subsequently heated at 70 °C for 12 h, washed thoroughly with deionized water and dried at 50 °C for 18 h. Elemental analysis gave Ni 18.76%, Al 4.44%, C 14.43%, N 0.20%, and H 4.10%, so the chemical composition of VBS/Ni−Al-LDH can be determined as $Ni_{0.66}Al_{0.34}(OH)_2(C_8H_7SO_3)_{0.31}(NO_3)_{0.03} \cdot 1.05H_2O$ (It should be noted that the water content was determined by TG-DTA analysis with the assumption that the interlayer water molecules totally disappear before 190 °C). As a comparison sample, nitrate intercalated Ni−Al-LDH was also prepared by the same method. PSS/Ni−Al-LDH sample was obtained after heating VBS/Ni−Al-LDH at 170 °C for 3 h.

Separation of the Polymerization Product (PSS) from LDH. The separation of the polymerization product of intercalated VBS from LDH was carried out by the following method: 2.0 g of PSS/Ni−Al-LDH powder was dissolved by adding 20 mL of 36% HCl and the solution was cooled in ice bath for 1 h to obtain yellow precipitation. The product was separated by filtration and washed thoroughly with anhydrous ethanol and dried under vacuum at 70 °C for 12 h.

Characterization. The sample of VBS/Ni−Al-LDH was characterized on a Rigaku D/MAX2500VB2+/PC X-ray diffractometer under air condition, using Cu Kα radiation (0.154184 nm) at 40 kV, 200 mA with a scanning rate of 5°/min, a step size of 0.02°/s, and a 2θ angle ranging from 3 to 70°.

The in situ high-temperature powder X-ray diffraction (in situ HT-XRD) measurements were performed on a Philip X'Pert Pro MPD X-ray diffractometer in the temperature range 30−580 °C under air condition, with Cu Kα radiation (0.154184 nm) operating at 40 kV, 40 mA. X'celerator was used for recording data. The heating rate was 30 °C/min with a holding time of 5 min before each measurement. Typical measurement conditions were in the 2θ range 4−70°; the step width is 0.0167° (2θ) and the step counting time is 20 s.

The in situ Fourier transform infrared (in situ FT-IR) spectra were recorded using a Nicolet 605 XB FT-IR spectrometer in the range 4000−400 cm^{-1} with 4 cm^{-1} resolution under air condition and a heating rate of 5 °C /min in the range from 30 to 290 °C. The standard KBr disk method (1 mg of sample in 100 mg of KBr) was used.

The solid UV−vis absorption spectra were collected in the range 210−800 nm on a Shimadzu U-3000 spectrophotometer, with the slit width of 1.0 nm. $BaSO_4$ was used as the reference.

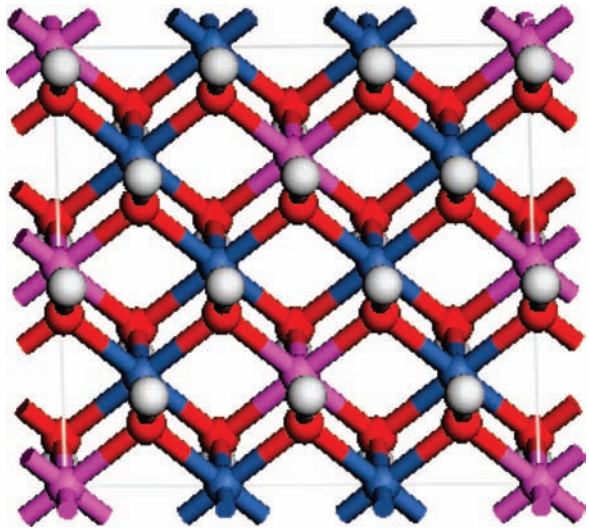

Figure 1. Layer model for Ni−Al-LDH (white, H; pink, Al; red, O; dark blue, Ni).

TG-DTA was measured on a PCT-1A thermal analysis system under ambient atmosphere with a heating rate of 10 °C/ min.

Analysis of metals was performed by ICP atomic emission spectroscopy on a Shimadzu ICPS-7500 instrument using solutions prepared by dissolving the samples in dilute nitric acid. Carbon, hydrogen, and nitrogen analyses were carried out using a Perkin-Elmer Elementarvario elemental analysis instrument.

The morphology of the polymerization product released from the PSS/Ni−Al-LDH composite was investigated by using a scanning electron microscope (SEM Hitachi S-3500) equipped with an EDX attachment (EDX Oxford Instrument Isis 300). The accelerating voltage applied was 20 kV. The thickness of the as-prepared polymer sheets was investigated by using the atomic force microscopy (AFM) (Digital Instruments).

Structural Model and Simulation Method. For the first step, an ideal LDH layer containing 8 Ni atoms and 4 Al atoms was built on the basis of each [AlO_6] octahedron surrounded by six [NiO_6] octahedra and each [NiO_6] octahedron, in turn, surrounded by three [AlO_6] octahedra, because the ratio of Ni to Al is 2:1, which ensures that Al atoms will not occupy adjacent octahedra. The lattice parameters of the 2-dimensional layer are $a = b = 3.03$ Å, which is in accordance with the literature[37] and our experimental results below. In this case, every octahedral layer has 12 metal atoms and 24 OH groups under the condition of $\alpha = \beta = 90°$, just as shown in Figure 1. On the basis of the model of the host layer, a supercell was constructed, with lattice parameters $a = b = 9.09$ Å and the initial interlayer spacing $c = 18$ Å, $\alpha = \beta = \gamma = 90°$ (equivalent to $4 \times 3 \times 1$ in the *a, b, c* directions). The supercell was treated as *P*1 symmetry and all of lattice parameters were considered as independent variables during the simulation. A 3-dimensional periodic boundary condition[38] was applied to the system, so the simulated supercell can be repeated infinitely in three directions. Then, for maintaining the whole system electrically neutral, four VBS monovalent anions and different numbers of water molecules were introduced into the simulated supercell randomly based on the rule that these molecules occupy the whole available interlayer space as much as possible. As a result, the formula of the simulated structures can be expressed as $Ni_8Al_4(OH)_{24}(C_8H_7SO_3)_4 \cdot nH_2O$.

We employed the modified cff91 force field, which was mentioned above, to perform MD simulation in the whole process. Force field parameters for Ni, Al, O and H in the layer

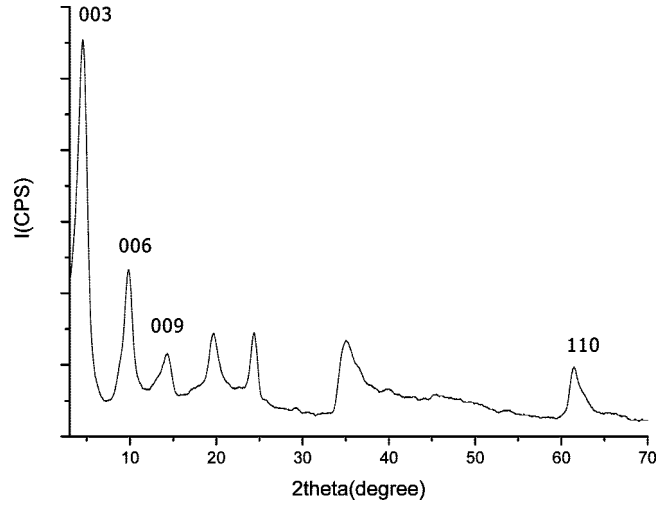

Figure 2. Powder XRD pattern of VBS/Ni−Al-LDH.

are derived from literature,[31] and QEq method[39] was used to calculate atomic charges of the layer, in which the partial charges are +0.813e for Ni, +1.688e for Al, −0.787e for O and +0.401e for H. Other force field parameters for the anions and water molecules were directly taken from the cff91 force field.[40] The Mulliken population analysis[41] was employed to calculate the partial charges of VBS anion and the polymerization product on HF/6-31G level using the Gaussian 03 programs.[42] For water molecule, the partial charges are taken from the single point charge (SPC) water model of Berendsen.[43] In potential energy calculations, the long-range Coulomb interactions between partial charges were computered by the Ewald summation technique[44] and a "spline cutoff" method was used to calculate van der Waals interaction. After energy minimization was applied on the initial models, MD simulations were performed in isothermal−isobaric (NPT) ensemble with the temperature of 300 K and the pressure of 0.1 MPa (about 1 atm). The Andersen method[45] and Parrinello−Rahman method[46] were used for controlling temperature and pressure, respectively.

The simulation time step was 1 fs and the total simulation time was 40 ps. The result shows that the system reached equilibrium with lattice parameters and total potential energy fluctuating around a constant value within the first 10 ps, as a result, during the remaining 30 ps, dynamic trajectories were recorded every 10 fs to analyze the ensemble average values, such as interlayer spacing and potential energy of the system. All of the simulations were performed using the Discover module in the Material Studio software package.[47]

Results and Discussion

1. Experimental Section. ***A. Crystal Structure of VBS intercalated Ni−Al-LDH.*** The powder XRD pattern of VBS/Ni−Al-LDH is shown in Figure 2. In this case, the reflections can be indexed to a hexagonal lattice with $R\bar{3}m$ rhombohedral symmetry, which is commonly used for the description of LDH structures. The main characteristic reflections of the VBS intercalated LDH appear at 4.52° (003), 9.86° (006), 14.3° (009) and 61.46° (110), respectively. The value of *c*, which stands for the interlayer spacing, is related to several factors (such as the size, orientation of interlayer anions and hydration state), and it can be calculated from averaging the positions of the three harmonics:

$$c = 1/3(d_{003} + 2d_{006} + 3d_{009}) = 1.88 \text{ nm}$$

It was found that the interlayer spacing in this work is a little larger than those of reported previously VBS/Ca−Al-LDH (1.77

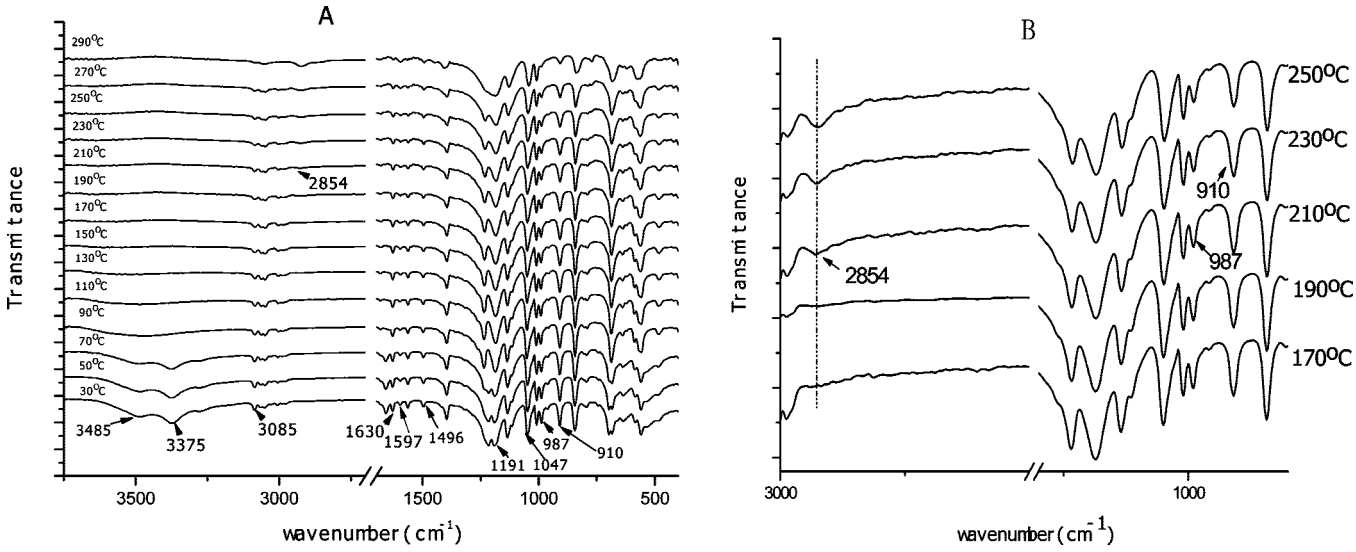

Figure 3. In situ FT-IR spectra for the thermal polymerization of VBS: (A) wavenumber from 4000 to 400 cm^{-1} in the range 30−290 °C every 20 °C; (B) selected regions for clarity in the range from 170 to 250 °C (the transmittance from 3000 to 1700 cm^{-1} is amplified 5 times).

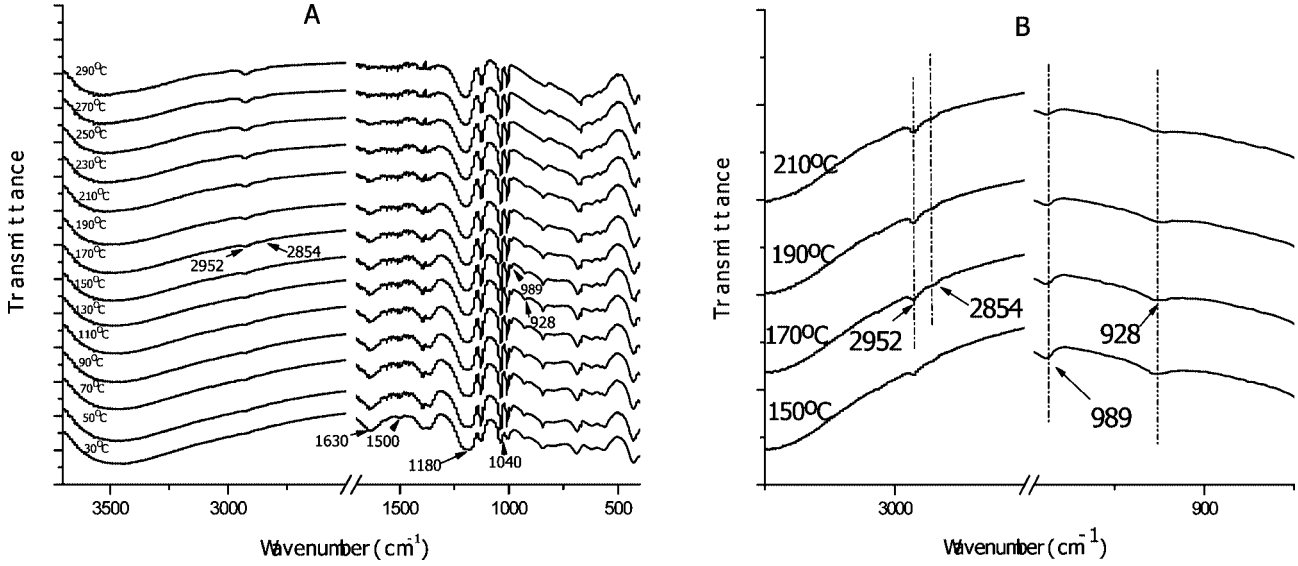

Figure 4. In situ FT-IR spectra for the thermal polymerization of VBS/Ni−Al-LDH: (A) wavenumber from 4000 to 400 cm^{-1} in the range 30−290 °C every 20 °C; (B) selected regions for clarity in the range from 150 to 210 °C.

nm)[16] and VBS/Zn−Al-LDH (1.82 nm).[17] Another value of the lattice parameter *a*, which stands for the distance of adjacent metal atoms in the LDH layers, can be calculated by $a = 2d_{110} = 3.02$ Å, in accordance with other Ni_2Al-LDH system (3.03 Å).[37] The values of *a* and *c* are referenced in the computer simulation section.

B. Thermal Polymerization of Pristine VBS and VBS/Ni−Al-LDH. To compare the thermal polymerization process between the pristine and intercalated VBS, the in situ FT-IR technique was performed for both VBS and VBS/Ni−Al-LDH with the temperature from 30 to 290 °C, and the spectra were recorded every 20 °C. Figure 3 shows the in situ FT-IR spectra of pristine VBS. At 30 °C, the bands at 3485 and 3375 cm^{-1} are attributed to the O−H stretching vibrations of the crystalline water molecule. The weak band at 3085 cm^{-1} corresponds to the stretching vibration of C−H in C═C−H and the bands at 987 and 910 cm^{-1} represent the out-of-plane bending of C−H with the type of RCH═CH_2 compound. The characteristic stretching vibrational band of C═C appears at 1630 cm^{-1}. The peaks at 1597 and 1496 cm^{-1} due to the skeleton vibration of benzene can also be observed. The symmetry and asymmetry absorption band of S═O in sulfonate are located at 1191 and 1047 cm^{-1} respectively.

With the temperature increasing, The O−H vibrations become broad at 90 °C and totally disappear when the temperature is above 110 °C, indicative of the loss of adsorbed water. As the temperature increases to 210 °C, the asymmetric C−H stretching vibration of −CH_2 appears at 2854 cm^{-1}; furthermore, the intensity of bands at 1630, 987, and 910 cm^{-1} decreases gradually in the range 210−290 °C. This indicates that thermal polymerization of VBS monomer occurs at ca. 210 °C. Other evidence can also be obtained by TG-DTA analysis discussed below.

In situ FT-IR spectra of VBS/Ni−Al-LDH are shown in Figure 4. At the temperature of 30 °C, characteristic absorption bands of VBS appear at 1630 and 1500 cm^{-1}, corresponding to the stretching vibration of C═C and the skeleton vibration of benzene respectively, which is similar to that of VBS analyzed above. Compared with pristine VBS, the bands of out-of-plane bending of C−H with the type of RCH═CH_2 shift to high frequency and appear at 989 cm^{-1} ($\Delta = 2$ cm^{-1}) and 928 cm^{-1} ($\Delta = 18$ cm^{-1}) respectively, whereas the absorption bands of

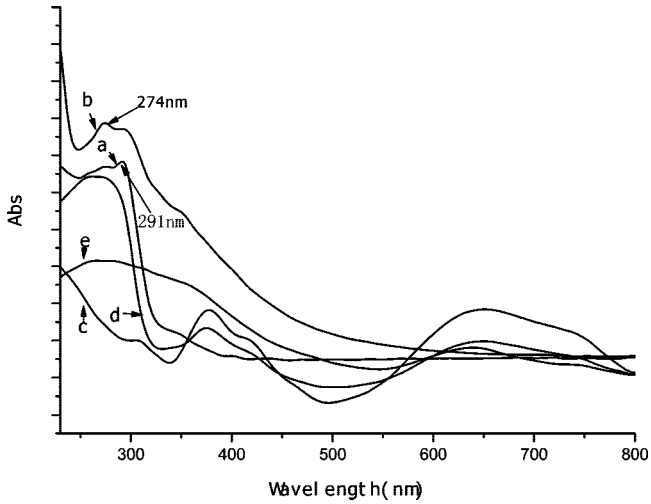

Figure 5. Solid UV−vis absorption spectra of different samples: (a) pristine VBS, (b) PSS obtained by heat treatment of pristine VBS at 210 °C, (c) NO_3^-/Ni−Al-LDH, (d) VBS/Ni−Al-LDH, and (e) PSS/Ni−Al-LDH obtained by heat treatment of the sample (d) at 170 °C.

sulfonate shift to low frequency located at 1180 cm^{-1} ($\Delta = -11$ cm^{-1}) and 1040 cm^{-1} ($\Delta = -7$ cm^{-1}), indicating the strong interactions between the sulfonate and hydroxyl layers. Finally, the lattice vibration of the inorganic layers appears in the range from 400 to 800 cm^{-1}.

As the temperature increases to ca. 170 °C, the intensity of band assigned to the symmetric C−H stretching vibration of $-CH_2$ (2952 cm^{-1}) increases obviously, moreover, the intensity of its asymmetric vibration peak (2854 cm^{-1}) increases slightly. In addition, the intensity of out-of-plane bending of C−H with the type of $RCH{=}CH_2$ (989 and 928 cm^{-1}) begins to decrease and nearly disappears at 250 °C. Therefore, it can be concluded that the intercalated VBS begins to polymerize at ca. 170 °C, 40 °C lower than that of the pristine VBS monomer. This can be possibly explained by the reason that the collision probability between monomer molecules increases when they are confined in 2D space. Malvaldi et al.[48] studied the diffusion-controlled stepwise polymerization kinetics in confined situations by a theoretical simulation method, and found that the polymerization rate was enhanced under the confined conditions. The results in this work are consistent with their theoretical simulation ones.

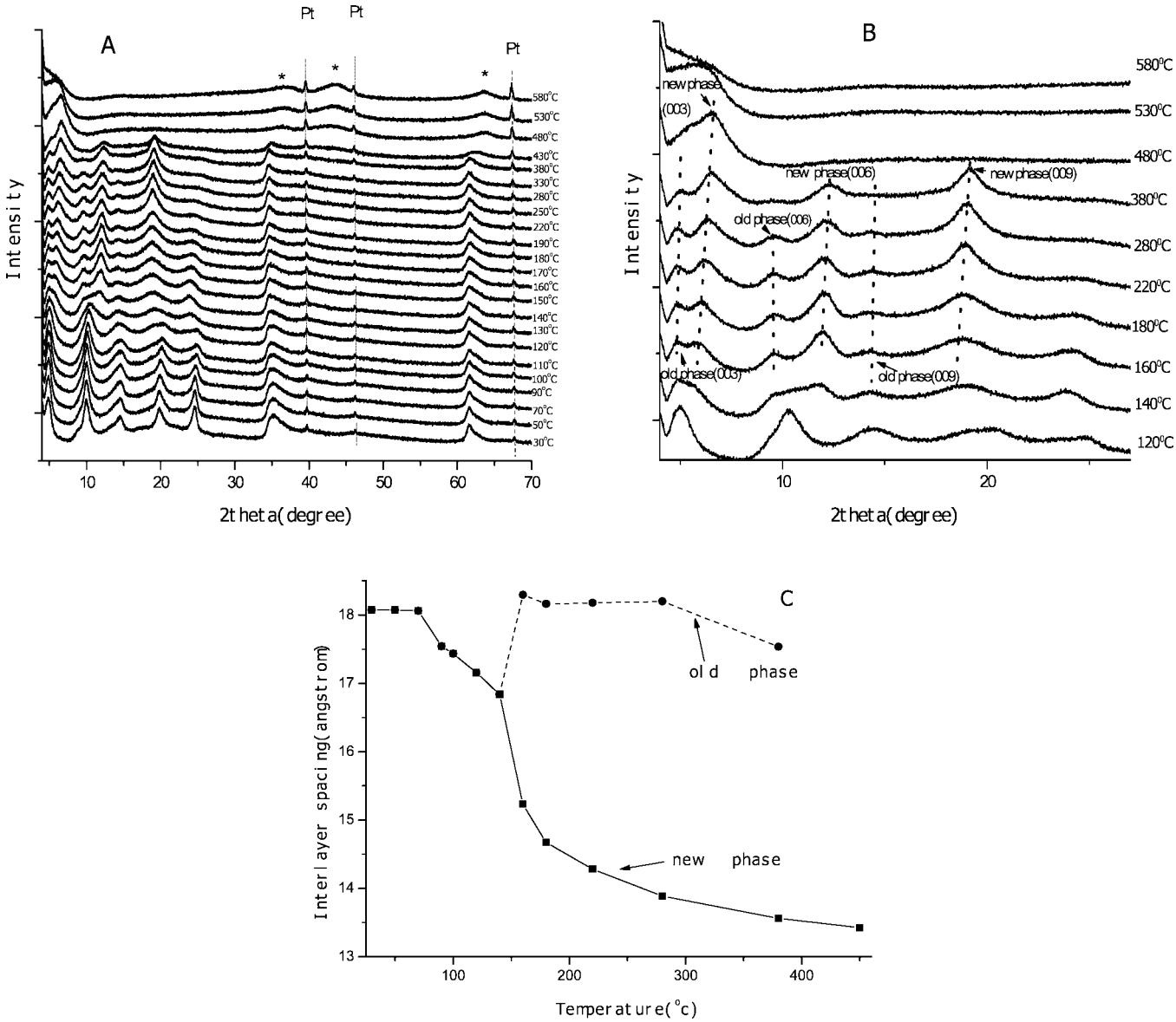

Figure 6. In situ XRD patterns of VBS intercalated Ni−Al-LDH in the temperature range 30−580 °C: (A) 2θ angular domain from 4 to 70° (*: NiO); (B) selected regions of low-2θ angular domain for clarity; (C) variation of the interlayer spacing with the increase of temperature.

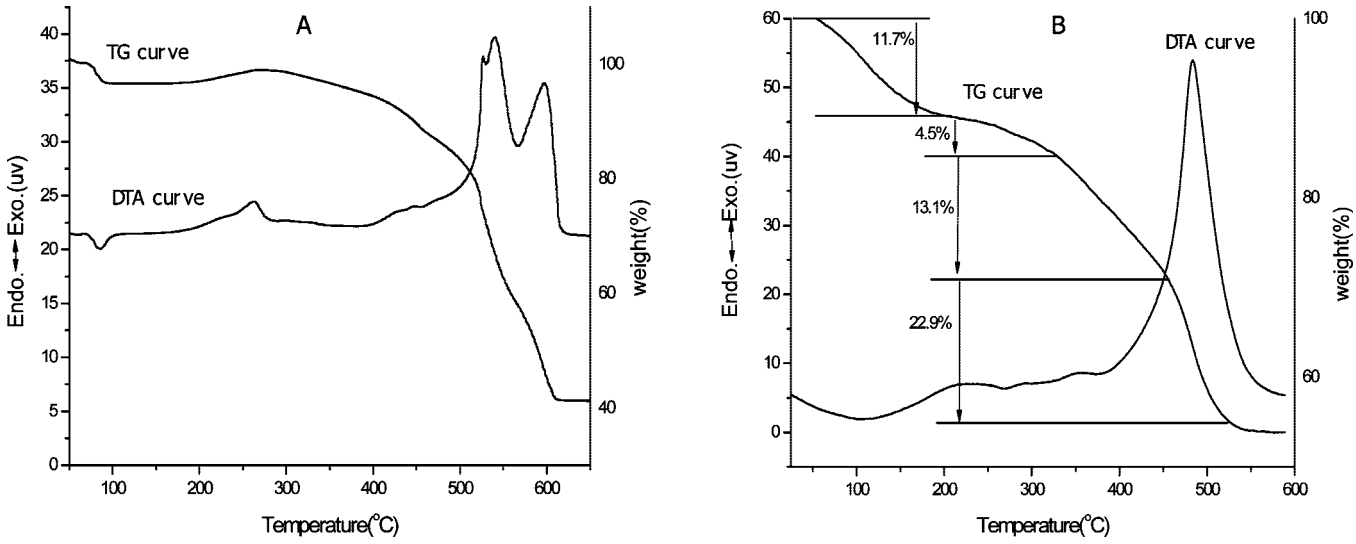

Figure 7. TG and DTA curves for (A) VBS and (B) VBS/Ni−Al-LDH.

The solid UV−vis spectra of different samples are displayed in Figure 5. The absorption band of VBS observed between 250 and 325 nm is attributed to the characteristic absorption of styrene. After VBS was thermally treated at 210 °C for 3 h, the maximum absorption peak shifts to high frequency by ca. 17 nm (from 291 to 274 nm), which is due to the polymerization of VBS. Compared with the spectrum of the NO_3^-/Ni−Al-LDH, a strong absorption band is observed between 250 and 300 nm for the sample of VBS/Ni−Al-LDH, due to the characteristic absorption of interlayer VBS. It should be noted that the main absorption band of VBS/Ni−Al-LDH shifts to high frequency by ca. 10−15 nm compared with that of pristine VBS, which is related to the host−guest interactions between the inorganic framework and VBS. After heat treatment at 170 °C for 3 h, the main absorption band of VBS/Ni−Al-LDH becomes broad and the absorption intensity between 250 and 300 nm decreases significantly. This may be attributed to the polymerization of VBS in the gallery of LDH.

The in situ high-temperature powder X-ray diffraction patterns of the intercalation product VBS /Ni−Al-LDH and the variation of the interlayer spacing in the temperature range 30−580 °C are shown in Figure 6. It can be observed that the (003) and (006) reflections of VBS/Ni−Al-LDH move to higher angle 2θ slightly from 30 to 140 °C, which is related to the deintercalation of interlayer water molecules. New reflections are observed at 5.8°, 11.9° and 24.3° as the temperature rises to 150 °C, corresponding to the (00*l*) reflections of the new phase for the polymerization product, i.e., PSS/Ni−Al-LDH; therefore, the polymerization temperature shown by in situ XRD is rather close to the result observed by in situ FT-IR spectra above (ca. 170 °C). The phase of VBS/Ni−Al-LDH coexists with the new one (PSS/Ni−Al-LDH) until the temperature increases to 430 °C. The reflection intensity of the VBS/Ni−Al-LDH decreases while that of the PSS/Ni−Al-LDH increases gradually in the range 150−430 °C, exhibiting a dynamic polymerization process of the sample. This phenomenon was seldom to be observed in other in situ polymerization reactions of monomer intercalated LDH, which implies that the thermal polymerization process of VBS/Ni−Al-LDH may be kinetically limited. At the temperature of 480 °C, the first appearance of broad reflections at about 36.2°, 42.8°, and 63.6° can be attributed to the phase of NiO, at the same time, the reflections associated with the LDH disappear. This is due to the decomposition of interlayer polymerization products and dehydroxylation of LDH layers, which will be further discussed in the next TG-DTA section.

Thermolysis of VBS was also studied as a reference sample to compare with VBS/Ni−Al-LDH, and its TG-DTA curves are displayed in Figure 7A. A weight loss occurs below 100 °C, with an endothermic peak in the DTA curve, which corresponds to the loss of crystalline water. It is surprising that the weight increases slightly from 210 to 300 °C with an exothermic peak, implying that the atmospheric oxygen participates in polymerization process. As we have known, the key role of oxygen in polymerization of interleaved aniline sulfonic acid has been demonstrated by Moujahid et al.[49] with in situ ESR measurements. The sharp weight loss between 500 and 620 °C is attributed to the decomposition and combustion of VBS. In the case of VBS/Ni−Al-LDH sample (Figure 7B), its thermal polymerization and decomposition process is characterized by four weigh loss steps. The first one from room temperature to 190 °C with an endothermic peak is due to the removal of surface adsorbed and interlayer water molecules. The second one with a gradual weight loss in the temperature range 190−350 °C, includes both the polymerization of VBS guest and the dehydroxylation of the brucit-like layers, accompanying with a slight exothermic peak from 180 to 260 °C in the DTA curve. The third and fourth ones are a combining process corresponding to the collapse of the layer and decomposition or combustion of VBS, with a strong exothermic peak at ca. 483 °C. Based on the comparison of their exothermic peak in the polymerization process, it was also found that the polymerization temperature of the intercalated VBS is lower than its pristine form, in agreement with the results of in situ FT-IR. Roland-Swanson et al.[13] has also observed this similar phenomenon in the system of SPMA/Zn−Al-LDH.

C. Morphology of the Interlayer Polymerization Product. The interlayer polymerization product of VBS at 170 °C was extracted by dissolving the layers of LDHs with acid treatment, and elemental analysis showed that no residual Ni and Al can be found in the polymerization product released from the host layers. Its FT-IR spectrum (see Supporting Information: Figure S1) was consistent with that of PSS, confirming the occurrence of interlayer polymerization reaction. SEM of the interlayer polymerization product (Figure 8) shows that it exhibits sheet-like morphology, due to the template effect of LDHs, whereas

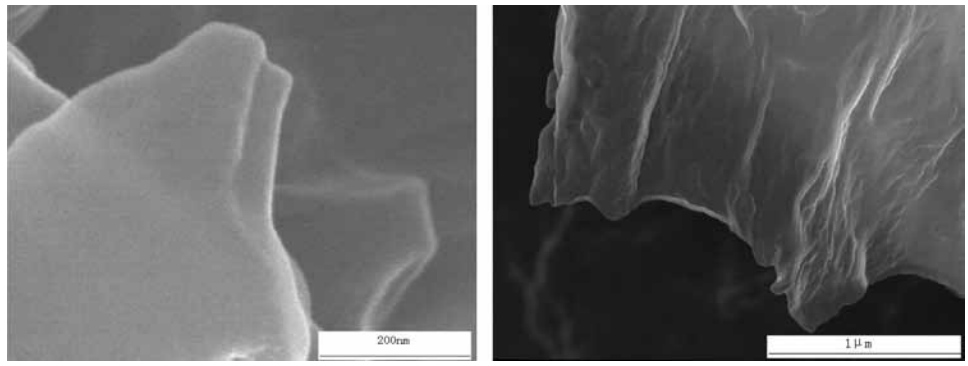

Figure 8. SEM images of PSS obtained by interlayer polymerization of VBS.

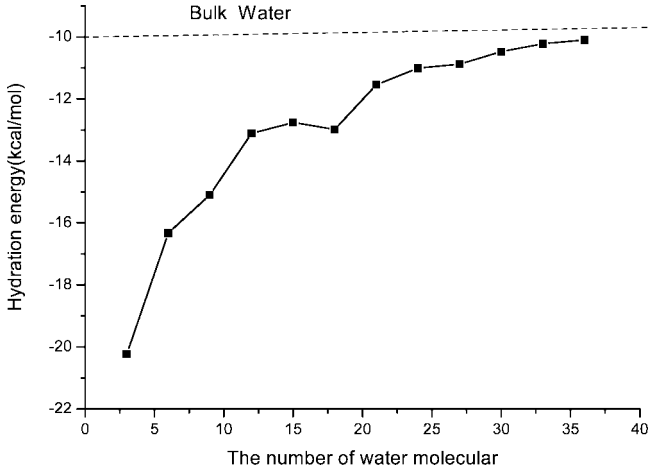

Figure 9. Hydration energy of VBS/Ni−Al-LDH with different water contents.

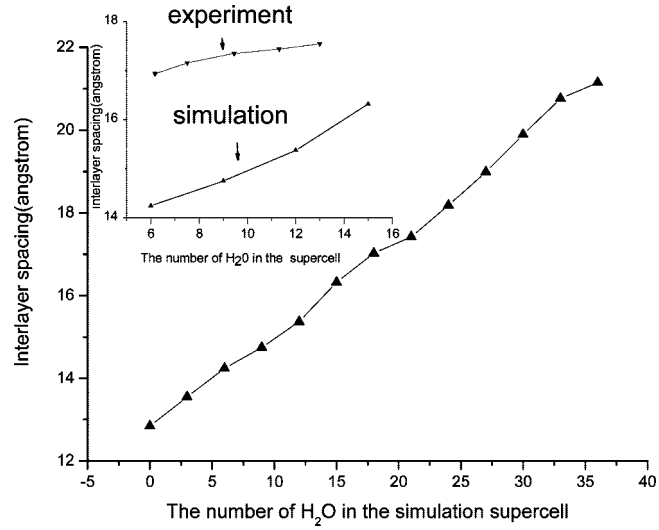

Figure 10. Variation of interlayer spacing as a function of the number of water for our model. Inset: the variation of interlayer spacing comparing the experiments with simulation results. The experimental results were obtained by in situ XRD, TG-DTA and elemental analysis, and the data were derived at the temperature of 90 °C, 100 °C, 110 °C, 120 °C, 130 °C.

no similar morphology of PSS was found in the bulk thermal polymerization of VBS (see Supporting Information: Figure S2). Therefore, this work provides a novel method to obtain polymers with special sheet-like morphology by the use of LDHs layers as template. The thickness of the PSS polymer sheets released from the host layers was further investigated by using the atomic force microscopy (AFM). It was found that the thickness is in the range ca. 10−30 nm (see Supporting Information: Figure S3), suggesting that the polymer sheets have aggregated or folded when they were removed from the interlayer region of Ni−Al-LDH.

2. Molecular Dynamics Simulation. ***A.. Hydration and Swelling Properties.*** As reported previously, the hydration energy is often used as an index to estimate the hydration behaviors and swelling properties of clays.[21–23,26,32,33] Although there are other hydration function expressions in views of thermodynamics,[21] the most common function form is defined as:

$$\Delta U = \frac{\langle U(N)\rangle - \langle U(0)\rangle}{N}$$

where N is the number of interlayer water molecules, $\langle U(N)\rangle$ is the average potential energy of hydrated clay containing N water molecules in the interlayer gallery and $\langle U(0)\rangle$ is the average potential energy of dry clay without interlayer water molecules.

The general trend of hydration energy in the system of VBS/Ni−Al-LDH is negative, and it increases upon the increase of the number of water (shown in Figure 9), which is similar to the results reported by other researchers for citrate and monocarboxylic acids intercalated Mg−Al-LDH with CLAYFF force field. [32,33] There is a relatively stable stage for hydration energy between 12 and 18 interlayer water molecules, implying that the water content in this range can mutually converse under different humidity conditions. It can be used to explain why the values of d_{003} are not consistent with each other slightly under different hydration conditions in experiment. In addition, it can be found that when a small energy barrier is passed through between the 18 and 21 water molecules, the hydration energy curve reaches another relatively stable stage, gradually approaching to the hydration energy value of SPC water (about −10 kcal/mol). Over the whole range, only one local minimum was found with 18 water molecules, which may correspond to a relatively preferred hydration state for VBS/Ni−Al-LDH. The experiment-determined water content was at the state with 13 water molecules, which is located in the stable range of hydration energy with n equal to 12−18.

Figure 10 shows that the simulated interlayer spacing is nearly linear with the water content, which is similar to the results of other anions intercalated Mg−Al-LDH.[24,31–33] As described in the Experimental Section, the molecular formula of the VBS/Ni−Al-LDH sample was determined by elemental analysis; the water content at a certain temperature as well as the process of dehydration were recorded by TG-DTA method; the interlayer spacing at certain temperature was obtained by in situ HT-XRD technique. As a result, comparison study between the experimental and simulated results for interlayer spacing with different hydration states was carried out. In addition, to eliminate the

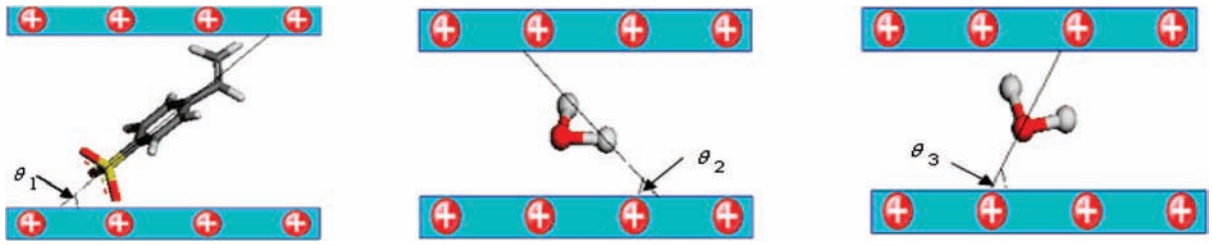

Figure 11. Three definitions of orientation angles. θ_1, θ_2, θ_3 stand for C_3 axis of sulfonate, H−H vector and dipole vector of water molecule relative to the host layers respectively.

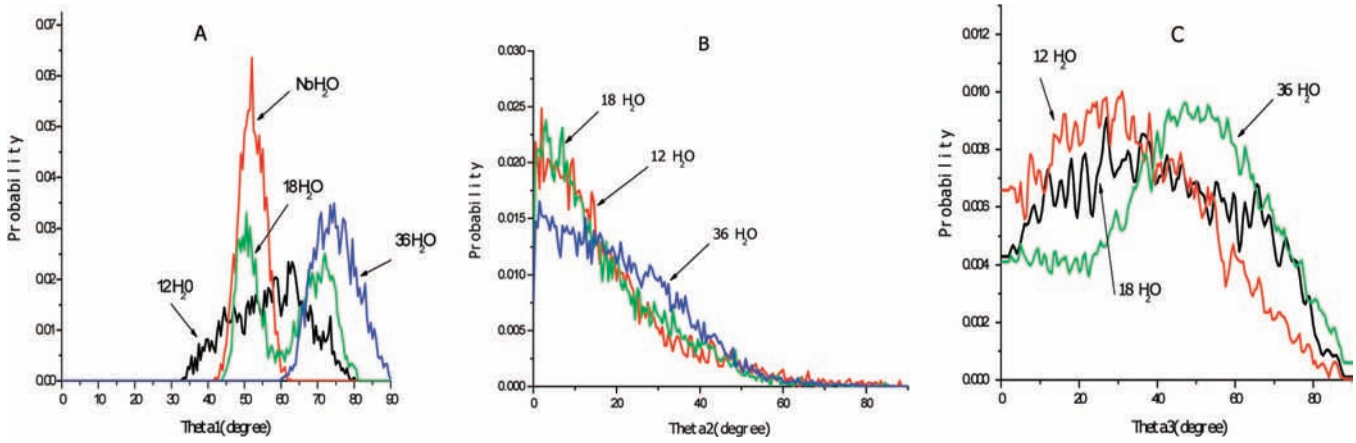

Figure 12. Distributions of three orientation angles under different hydration conditions.

influences of surface adsorbed water and the polymerization process, temperature range of 90−130 °C was chosen to make the comparison (shown in the inset of Figure 10).

It can be known from Figure 10 that the simulated interlayer spacing with the experimental hydration state is systematically lower than that of experimental value by ca. 2 Å. Another important piece of information is that the experimental variation of interlayer spacing under different hydration conditions is not so obvious as that of the simulation one. Linear regression analysis shows that the simulated interlayer spacing increases by about 0.23 Å upon increasing one interlayer water molecule in our model, which is about 2 times of the experimental result. This implies that the host−guest interaction in real system is stronger than that of our ideal model. The differences between the experimental and computational results may be attributed to the reasons as follows: First, for such a complex LDH system, the experimental structure of VBS/Ni−Al-LDH cannot be as perfect a crystal model as our simple theoretical one; e.g., there may be some lattice defects and different stacking modes of the layers in the real system. Furthermore, a small amount of cointercalated nitrates in the gallery of LDH can also lead to the deviation of interlayer spacing. Second, in our simulation process, the parameters of atomic charges or Lennard-Jones potentials in the cff91 force field can also influence the calculation of the interaction, and it is known that a stronger attraction between the layer and anions leads to a lower interlayer spacing. Last, but not least, because the hydration state can converse in the range $n = 12-18$ for interlayer water molecules and the calculated interlayer spacing is sensitive to the water content, the experiment-determined hydration state may also be responsible for the error. It should be pointed out that the simulation temperature is not a key factor affecting the calculated results deviated from the real system, because the calculated interlayer spacing at 400 K is only larger than that of at 300 K by at most 0.09 Å for the VBS/Ni−Al-LDH system under different hydration conditions. To investigate the discrepancy of interlayer spacing influenced by partial charges of the guest molecule, partial atomic charges of VBS anion were recalculated by the more robust Merz−Kollmann (MK) scheme at the HF/6-31 g** level with other computational conditions remaining unchanged. We performed the MD method for the VBS/Ni−Al-LDH (0 and 18 H_2O) system. The results show that the interlayer spacings of VBS/Ni−Al-LDH with 0 water and 18 water are 13.06 Å ($\Delta = 0.21$ Å) and 16.94 Å ($\Delta = -0.08$ Å), respectively, which are very close to the values calculated by Mulliken population analysis (12.85 and 17.02 Å for 0 and 18 water, respectively). This suggests that the interlayer spacings for the two states are almost independent of the computational method of the guest molecule and the partial atomic charge may play a less important role than expectation. Actually, the ionic hydroxide layer could polarize the interlayer molecules up to a considerable extent and the partial charges of the interlayer VBS may be different from those of pristine one.

B. Structures of Guest Molecules between the Layers. The interlayer arrangements and orientations of the guest molecules are important information to understand the host−guest structures. In this section, three orientation angles were defined to describe the geometries of guest molecules (shown in Figure 11): the angle θ_1 stands for the orientation angle of C_3 axis of sulfonate, which is also the C_2 axis of benzene, with respect to the layers; the angle θ_2 stands for the orientation angle of H−H vector of water molecule with respect to the layers; the angle θ_3 stands for the orientation angle of dipole vector of water molecule with respect to the layers. The orientation angles mentioned above in different hydration states were probed.

Figure 12A displays the distribution of θ_1 under four typical hydration conditions. The orientation varies between 42 and 60° and exhibits nearly normal distribution in anhydrous situation. Under this condition, all of the guest molecules are inclining to the layers, which can be attributed to the strong electrostatic interactions between the cationic host layers and the anionic

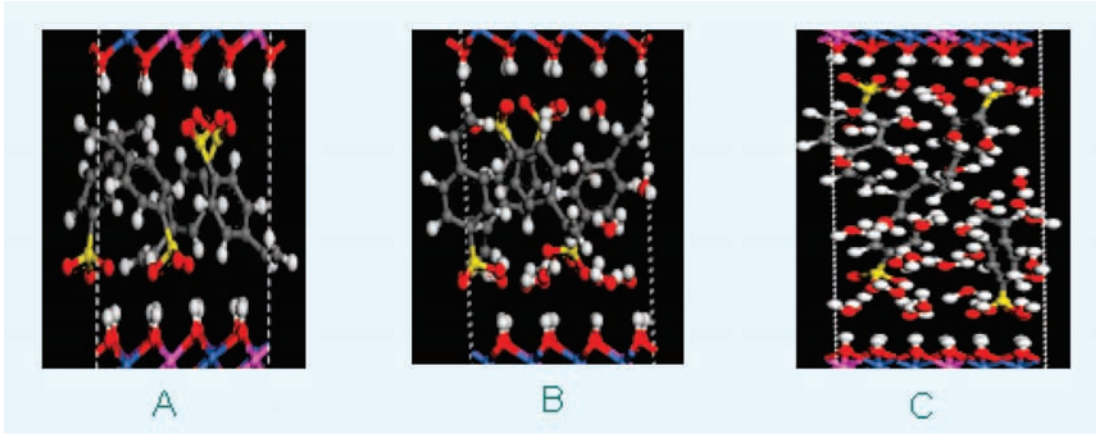

Figure 13. Snapshots of the simulation for VBS intercalated Ni−Al-LDH under three different hydration conditions: (A) without water; (B) 12 water; (C) 36 water.

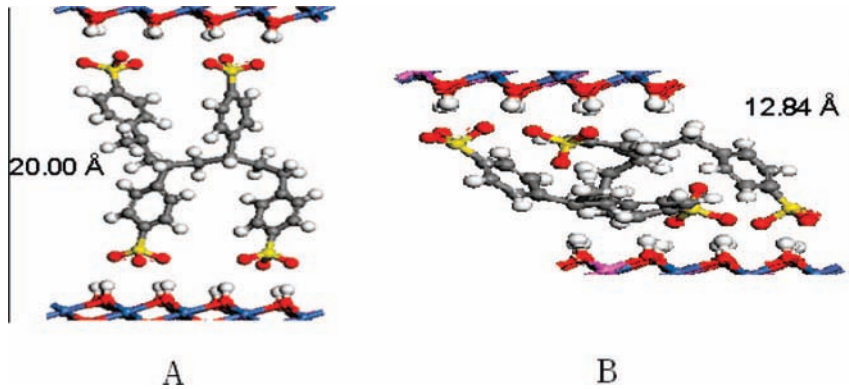

Figure 14. Snapshots of initial and equilibrium configurations for the tetramer of VBS intercalated Ni−Al-LDH: (A) initial structure (d_{003} = 20.00 Å); (B) equilibrium structure (d_{003} = 12.84 Å).

guest molecules. When the molar ratio of water and VBS is 3:1 (12 water molecules between the layers in our model, approximately corresponding to the experimental hydration state), the distribution of θ_1 broadens. A less tilted angle distribution between 30 and 40° and a more tilted one between 60 and 80° appeared. When the molar ratio of water and VBS increases to 4.5:1 (18 water molecules in the layers), it can be observed that there are two preferred orientations for VBS between the layers, one of which is similar to that of the anhydrous condition, another angle is mainly populated in the range 60−80°. Compared with the distribution with 12 interlayer water molecules, the preferred orientation near 60° disappears, so this state can be attributed to a transition from low water content to high content. Moreover, it can be concluded that this state is relatively stable on the basis of the results of hydration energy for VBS/Ni−Al-LDH. A rather slow increase in the interlayer spacing from 18 to 21 interlayer water can be observed, which also suggests that the model with 18 interlayer water is a stable state. As the molar ratio of water and VBS increases to 9:1 (36 water between the layers), the angle distribution less than 60° disappears and the one from 80 to 90° is observed, indicating that the VBS molecules are nearly perpendicular to the host layers. It can be concluded that the guest molecules have a tendency from tilted to vertical arrangement with respect to the layers as the interlayer water increases.

Figure 12B exhibits the distribution of orientation angle for H−H vector of water molecule relative to the layers under three hydration conditions. The distribution from 0 to 60° represents an exponential decay and the distribution from 60 to 90° almost does not appear under each hydration state, which is similar to the simulation results of SO_4^{2-}/LDH system.[31] There is no obvious difference in the distribution state between 12 and 18 water molecules. However, when the number of water increases to 36, the angle from 0 to 20° exhibits approximately uniform distribution compared with that of low water content condition. It can be known that H−H vector is parallel to the layers mostly which can meet the condition of force equilibrium in different hydration states.

Figure 12C displays the distribution of orientation angle for dipole vector of water relative to the layers, which is in the range from 0 to 90°. The maximum likelihood angle appears at nearly 30° with 12 and 18 interlayer water and it shifts to higher angle direction (ca. 50°) as the interlayer water increases to 36. This suggests that with the increase of water content, the plane of water molecules becomes more tilt relative to the layers although the state that the plane parallel to layers can also be found in each state.

Figure 13 shows snapshots of the simulation for VBS intercalated Ni−Al-LDH in three different hydration states, which can help to further understand the structure and orientation of VBS in the gallery of Ni−Al-LDH. It can be qualitatively seen that the guest molecules exhibit monolayer arrangement mode in low water content and nearly bilayer arrangement mode in high water content. Moreover, the styrene groups of VBS have a trend to stack in the intermediate position between the layers, which corresponds to the hydrophobic region and nonpolar environment in the gallery of LDH, whereas the sulfonate groups mainly occupy the two ends of the layers, which is the hydrophilic region and polar environment.

C. Model of Tetramer intercalated Ni−Al-LDH. A model for tetramer of VBS intercalated Ni−Al-LDH was investigated (shown in Figure 14) and the initial configuration was chosen, similar to the structural model of PSS intercalated Ca−Al-LDH as Vieille et al. suggested.[16] No water molecule was presented in the layers, and the calculated equilibrium interlayer spacing was 12.84 Å. We also performed MD simulations for this model at 500 and 600 K, and the interlayer spacing varied from 12.91 to 12.96 Å, which is consistent with the experimental result of in situ HT-XRD for VBS/ Ni−Al-LDH in the range from 280 to 330 °C (about 13.68 to 13.88 Å).

Conclusion

In this work, the polymerization reaction of 4-vinylbenzenesulfonic anion (VBS) in the 2D layers of Ni−Al-LDH has been investigated. Thermal polymerization of VBS monomer occurs at ca. 210 °C, whereas the intercalated VBS begins to polymerize at ca. 150−170 °C. This indicates that the polymerization of VBS monomer occurs more easily between the layers of LDH upon heating, which can be attributed to the increase in collision probability between molecules when they are confined in 2D space. The coexistence of VBS/Ni−Al-LDH and PSS/Ni−Al-LDH in the temperature range 150−430 °C was observed by in situ HT-XRD, which implies the thermal polymerization process of VBS/Ni−Al-LDH is kinetically limited. Furthermore, the polymerization product (PSS) with sheet-like morphology was released from the host matrix with the layers of LDHs as template.

Molecules dynamics simulation was employed to study the structures and arrangements of guest molecules in the gallery of Ni−Al-LDH. Hydration energies have been calculated first and there are two relatively stable stages as the number of interlayer water increases, indicating that the hydration state of the system can mutually converse under different humidity conditions at certain stage. The interlayer spacing of different hydration states was investigated in terms of both experiment and computer simulation. The experiment-determined interlayer spacing is less affected by interlayer water molecule than the simulated one, which suggests that the host−guest interaction between the layers and VBS molecules in the real state is stronger than that of the model system. To probe the arrangement styles of guest molecules, three orientation angles have been defined. VBS exhibits a tendency from tilt to vertical arrangement with respect to the layers with the increase of interlayer water content. For water molecules, the state that the plane parallel to the inorganic layer can be found and they become more inclined to the layers upon increasing the water content. A typical tetramer of VBS intercalated LDH was selected as the model of polymerization product and the computational equilibrium interlayer spacing fits well with the experimental result of in situ HT-XRD.

Therefore, by virtue of combination of experiment and theoretical calculation, this work gives a more detailed investigation on the thermal polymerization of guest monomers confined in the layers of Ni−Al-LDH, and provides a further understanding of the arrangement styles as well as orientations of monomers and products confined between the sheets of LDHs. It can be expected that the layered inorganic materials like LDHs, could be applied to impose restricted geometry on the interlayer confined reaction leading to enhanced control of product morphology and distribution.

Acknowledgment. This work was supported by the National Natural Science Foundation of China, the Program for New Century Excellent Talents in University (Grant No.: NCET-05-121), the 111 Project (Grant No.: B07004) and the Program for Changjiang Scholars and Innovative Research Team in University (Grant No.: IRT0406).

Supporting Information Available: FT-IR spectra of the polymerization product released from the interlayer region of LDH as well as PSS (Figure S1). SEM image of the thermal polymerization product of pristine VBS (Figure S2). Tapping-mode AFM image of the polymer sheets removed from the interlayer region of LDH (Figure S3). This material is available free of charge via the Internet at http://pubs.acs.org.

References and Notes

(1) Constantino, V. R. L.; Pinnavaia, T. J. *Catal. Lett.* **1994**, *23*, 361.
(2) Corma, A.; Fornes, V.; Rey, F.; Cervilla, A.; Llopis, E.; Ribera, A. *J. Catal.* **1995**, *152*, 237.
(3) Fogg, A. M.; Green, V. M.; Harvey, H. G.; O'Hare, D. *Adv. Mater.* **1999**, *11*, 1466.
(4) Fogg, A. M.; Dunn, J. S.; Shyu, S. G.; Cary, D. R.; O'Hare, D. *Chem. Mater.* **1998**, *10*, 351.
(5) Khan, A. I.; Norquist, A. J.; O'Hare, D. *Chem. Commun.* **2001**, 2342.
(6) Choy, J. H.; Jung, J.; Oh, S. J. M.; Park, M.; Jeong, J.; Kang, Y. K.; Han, O. J. *Biomaterials* **2004**, *25*, 3059.
(7) Ogawa, M.; Kuroda, K. *Chem. Rev.* **1995**, *95*, 399.
(8) Tagaya, H.; Sato, S.; Kuwahara, T.; Kadokawa, J.; Masa, K.; Chiba, K. *J. Mater.Chem.* **1994**, *4*, 1907.
(9) Venugopal, B. R.; Ravishankar, N.; Perrey, C. R.; Shivakumara, C.; Rajamathi, M. *J. Phys. Chem. B* **2006**, *110*, 772.
(10) Wei, M.; Shi, Z. Y.; Evans, D. G.; Duan, X. *J. Mater. Chem.* **2006**, *16*, 2102.
(11) Schöllhorn, R. *Chem. Mater.* **1996**, *8*, 1747.
(12) Moujahid, E. M.; Dubois, M.; Besse, J.-P.; Leroux, F. *Chem. Mater.* **2005**, *17*, 373.
(13) Roland-Swanson, C.; Besse, J.-P.; Leroux, F. *Chem. Mater.* **2004**, *16*, 5512.
(14) Vaysse, C.; Guerlou-Demourgues, L.; Duguet, E.; Delmas, C. *Inorg. Chem.* **2003**, *15*, 4559.
(15) Moujahid, E. M.; Besse, J.-P.; Leroux, F. J. *Mater. Chem.* **2002**, *12*, 3324.
(16) Vieille, L.; Taviot-Gueho, C.; Besse, J.-P.; Leroux, F. *Chem. Mater.* **2003**, *15*, 4369.
(17) Moujahid, E. M.; Dubois, M.; Besse, J.-P.; Leroux, F. *J. Mater. Chem.* **2003**, *13*, 258.
(18) Leroux, F.; Raymundo-Piñero, E.; Nedeleca, J.-M.; Béguin, F. *J. Mater. Chem* **2006**, *16*, 2074.
(19) Greenwell, H. C.; Jones, W.; Peter, V. C.; Stackhouse, S. *J. Mater. Chem.* **2006**, *16*, 708.
(20) Boek, E. S.; Coveney, P. V.; Skipper, N. T. *J. Am. Chem. Soc.* **1995**, *117*, 12608.
(21) Hensen, E. J. M.; Smit, B. *J. Phys. Chem. B* **2002**, *106*, 12664.
(22) Smith, D. E. *Langmuir* **1998**, *14*, 5959.
(23) Aicken, A. M.; Bell, I. S.; Coveney, P. V.; Jones, W. *Adv. Mater.* **1997**, *9*, 496.
(24) Newman, S. P.; Williams, S. J.; Coveney, P. V.; Jones, W. *J. Phys. Chem. B* **1998**, *102*, 6710.
(25) Titiloye, J. O.; Skipper, N. T. *Chem. Phys. Lett.* **2000**, *329*, 23.
(26) Wang, J. W.; Kalinichev, A. G.; Kirkpatrick, R. J.; Hou, X. Q. *Chem. Mater.* **2001**, *13*, 145.
(27) Kalinichev, A. G.; Kirkpatrick, R. J. *Chem. Mater.* **2002**, *14*, 3539.
(28) Cygan, R. T.; Liang, J. J.; Kalinichev, A. G. *J. Phys. Chem. B* **2004**, *108*, 1255.
(29) Mohanambe, L.; Vasudevan, S. *Langmuir* **2005**, *21*, 10735.
(30) Mohanambe, L.; Vasudevan, S. J. *Phys. Chem. B* **2005**, *109*, 15651.
(31) Li, H.; Ma, J.; Evans, D. G.; Zhou, T.; Li, F.; Duan, X. *Chem. Mater.* **2006**, *18*, 4405.
(32) Kumar, P. P.; Kalinichev, A. G.; Kirkpatrick, R. J. *J. Phys. Chem. B* **2006**, *110*, 3841.
(33) Kumar, P. P.; Kalinichev, A. G.; Kirkpatrick, R. J. *J. Phys. Chem. C* **2007**, *111*, 13517.
(34) Mayo, S. L.; Olafson, B. D.; Goddard, W. A. *J. Phys. Chem.* **1990**, *94*, 8897.
(35) Kalinichev, A. G.; Kirkpatrick, R. J.; Cygan, R. T. *Am. Mineral.* **2000**, *85*, 1046.
(36) Beneke, M. M. K.; Lagaly, G. *Inorg. Chem.* **1990**, *29*, 5201.
(37) Hernandez-Moreno, M. J. H.; Ulibarri, M. A.; Rendon, J. L.; Serna, C. J. *Phys. Chem. Miner.* **1985**, *12*, 34.

(38) Leach, A. R. *Molecular Modeling, Principles and Applications*, 2nd ed.; Pearson Education Ltd.: England, 2001.

(39) Rappé, A. K.; Goddard, W. A. J. *Phys. Chem.* **1991**, *95*, 3358.

(40) Maple, J. R.; Hwang, M.-J.; Stockfisch, T. P.; Dinur, U.; Waldman, M.; Ewig, C. S.; Hagler, A. T. *J. Comput. Chem.* **1994**, *15*, 162.

(41) Mulliken, R. S. *J. Chem. Phys.* **1955**, *23*, 1833.

(42) Frisch, M. J.; Trucks, G. W.; Schlegel, H. B.; Scuseria, G. E.; Robb, M. A.; Cheeseman, J. R., Montgomery, J. A., Jr.; Vreven, T.; Kudin, K. N., Burant, J. C.; Millam, J. M.; Iyengar, S. S.; Tomasi, J.; Barone, V.; Mennucci, B.; Cossi, M.; Scalmani, G.; Rega, N.; Petersson, G. A.; Nakatsuji, H.; Hada, M.; Ehara, M.; Toyota, K.; Fukuda, R.; Hasegawa, J.; Ishida, M.; Nakajima, T.; Honda, Y., Kitao, O.; Nakai, H.; Klene, M.; Li, X.; Knox, J. E.; Hratchian, H. P.; Cross, J. B.; Adamo, C.; Jaramillo, J.; Gomperts, R.; Stratmann, R. E.; Yazyev, O.; Austin, A. J.; Cammi, R.; Pomelli, C.; Ochterski, J. W.; Ayala, P. Y.; Morokuma, K.; Voth, G. A.; Salvador, P.; Dannenberg, J. J.; Zakrzewski, V. G.; Dapprich, S.; Daniels, A. D.; Strain, M. C.; Farkas, O.; Malick, D. K.; Rabuck, A. D.; Raghavachari, K.; Foresman, J. B.; Ortiz, J. V.; Cui, Q.; Baboul, A. G.; Clifford, S.; Cioslowski, J.; Stefanov, B. B.; Liu, G.; Liashenko, A.; Piskorz, P.; Komaromi, I.; Martin, R. L.; Fox, D. J.; Keith, T.; Al-Laham, M. A.; Peng, C. Y.; Nanayakkara, A.; Challacombe, M.; Gill, P. M. W.; Johnson, B.; Chen, W.; Wong, M. W.; Gonzalez, C.; Pople, J. A. *Gaussian 03*, revision B.04, Gaussian, Inc.: Pittsburgh, PA, 2003.

(43) Berendsen, H. J. C.; Postma, J. P. M.; van Gunsteren, W. F.; Hermans, J., *Interaction models for water in relation to protein hydration. In Intermolecular Forces*; Pullman, B.,. Ed.; Riedel, Dordrecht, The Netherlands, 1981; p 331.

(44) Allen, M. P.; Tildesley, D. J. *Computer Simulation of Liquids*; Clarendon: Oxford, U.K., 1987.

(45) Andersen, H. C. *J. Chem. Phys.* **1980**, *72*, 2384.

(46) Parrinello, M.; Rahman, A. *J. Appl. Phys.* **1981**, *52*, 7182.

(47) *Discover Module, MS Modeling*, version 2.2, Accelrys Inc.: San, Diego, CA, 2003.

(48) Malvaldi, M.; Bruzzone, S.; Picchioni, F. *J. Phys. Chem. B* **2006**, *110*, 12281.

(49) Moujahid, E. M.; Dubois, M.; Besse, J.-P.; Leroux, F. *Chem. Mater.* **2002**, *14*, 3799.

JP801922B